Auditory corticofugal neurons transmit non-auditory signals to support discriminative learning

Alexander N. Ford[1#], Jordyn E. Czarny[1#], Meike M. Rogalla[1], Gunnar L. Quass[1], & Pierre F. Apostolides[1,2]*
1) Kresge Hearing Research Institute, Department of Otolaryngology/Head & Neck Surgery
2) Department of Molecular and Integrative Physiology
University of Michigan Medical School
*corresponding author: piaposto@med.umich.edu
#Equal Contribution

Abstract

Layer 5 pyramidal neurons of sensory cortices project "corticofugal" axons to myriad of sub-cortical targets, thereby broadcasting high-level signals important for perception and learning. Recent studies suggest *dendritic Ca^{2+} spikes* as key biophysical mechanisms supporting corticofugal neuron function: These long-lasting events drive burst firing, thereby initiating uniquely powerful signals to modulate sub-cortical representations and trigger learning-related plasticity. However, the behavioral relevance of corticofugal dendritic spikes is poorly understood. We shed light on this issue using 2-photon Ca^{2+} imaging of auditory corticofugal dendrites as mice engage in a sound-discrimination task. Unexpectedly, only a minority of dendritic spikes were triggered by sound. Rather, task-related dendritic activity mostly occurred following sound termination and reflected mice's instrumental actions, irrespective of reward consumption. Temporally selective silencing of this motor-related activity impaired auditory discrimination learning. Thus, corticofugal systems' contribution to learning and plasticity may be largely motor, rather than sensory in nature.

Introduction

A ubiquitous circuit motif of the neo-cortex is that layer 5 "corticofugal" pyramidal neurons send axons to multiple sub-cortical regions, thereby broadcasting cortical computations throughout the brain (Usrey and Sherman, 2019; Sherman and Usrey, 2021). Consequently, these descending pathways enable a predictive or feedback control of hierarchically lower circuits that influences learning and behavior across multiple time scales (Bajo et al., 2010; Liu et al., 2016; Takahashi et al., 2016, 2020; Ranganathan et al., 2018; Doron et al., 2020; Ruediger and Scanziani, 2020). Interestingly, corticofugal neurons generate two distinct types of action potential patterns: Low frequency (1-50 Hz) simple spike trains, and powerful high frequency bursts (100-200 Hz) driven by a long-lasting, regenerative Ca^{2+} spike initiated in the apical dendrites (Larkum et al., 1999; Harnett et al., 2013; Slater et al., 2013; Beaulieu-Laroche et al., 2019; Fletcher and Williams, 2019; Lacefield et al., 2019; Galloni et al., 2020). Because the neo-cortex is suggested to transmit information via a rate code (Banerjee et al., 2008; London et al., 2010), such burst firing may be a highly salient output signal with important downstream consequences. Indeed, given the low release probability of central nerve terminals (Borst, 2010; Scimemi and Diamond, 2012; Miki et al., 2018), spike bursts will be more effectively transmitted to downstream targets compared to low-frequency spike trains (Lisman, 1997; Tsodyks and Markram, 1997; Xu et al., 2012b; Apostolides et al., 2016). Burst firing could thus enable pyramidal neurons to transmit unique signals multiplexed with distinct information encoded in simple spike trains, thereby increasing the computational flexibility of cortical circuits (Naud and Sprekeler, 2018). However, the behavioral relevance of dendritic spikes is unclear, owing to the difficulty of recording dendritic activity in actively engaged animals.

We address this knowledge gap using 2-photon Ca^{2+} imaging of layer 5 corticofugal neuron dendrites in auditory cortex of mice performing a reward-based sound discrimination task. We used a retrograde adeno-associated virus (AAV; Tervo et al., 2016) to express the Ca^{2+} indicator GCaMP6f in auditory corticofugal neurons projecting to the inferior colliculus (IC), a major midbrain hub that integrates ascending auditory brainstem signals with descending feedback from auditory cortex (Morest and Oliver, 1984; Winer et al., 1998; Oberle et al., 2022). Interestingly most auditory corticofugal dendrites were *inhibited* by sound, with a subset of neurons generating dendritic spikes primarily in response to sounds predicting reward availability. Instead the majority of task-related dendritic activity followed sound termination and was triggered primarily by mice's operant licking behavior, independent of reward consumption. Temporally selective silencing of motor-related activity in corticofugal neurons impaired discriminative auditory learning. Our results reveal a surprising non-sensory contribution of auditory cortex to learned behaviors. The data suggest that cortical motor activity recruits plasticity mechanisms, either in corticofugal neurons or their downstream targets, to stamp in learned associations between sensory signals and instrumental actions.

Results

Head-fixed mice discriminate sound temporal envelope fluctuations in a GO/NO-GO paradigm

Water-deprived, head-fixed mice (n=14) were trained to report the presence or absence of sinusoidal amplitude-modulation (**sAM**; 15 Hz modulation rate, 100% modulation depth, 1 s duration) in a 2-octave band-limited noise carrier (4-16 kHz; 65-70 dB SPL). On 50% of trials, a GO sound instructed that licking a waterspout during an answer period following sound offset would deliver a drop of 10% sugar water. In the other half of trials, a NO-GO sound instructed to withhold licking; incorrect licks during the answer period (false alarms) were punished with an increased inter-trial interval (Figure 1A). Whether the sAM sound served as GO or NO-GO was counterbalanced across mice (n=7 mice in each group). Mice rapidly learned associations between the GO sound and reward delivery, as evidenced by a consistently high hit rate even during the first five training sessions (Figure 1B). The number of false alarms gradually fell across training, such that mice's sensitivity index (d-prime) increased with continued training primarily due to an increased propensity of withholding responses on NO-GO trials (Figure 1C). Thus, head-fixed mice rapidly learned to attend to, and subsequently discriminate, the temporal envelope of sounds.

Diverse activity profiles of auditory corticofugal dendritic spikes in behaving mice

The IC of the midbrain receives major descending projections from the auditory cortex, with 80-90% of the auditory cortico-collicular pathway arising from thick-tufted layer 5 pyramidal neurons (Winer et al., 1998; Schofield, 2009; Slater et al., 2013; Williamson and Polley, 2019; Yudintsev et al., 2021; Lesicko et al., 2022). Thus, we expressed the Ca^{2+} indicator GCaMP6f and a nuclear localized tdTomato in auditory corticofugal neurons via a retrograde AAV injected into the left IC (Figure 1D). Labeling in auditory cortex was restricted to layer 5 pyramidal neurons (Figure 1E), in agreement with the known tropism of rAAV2-retro (Tervo et al., 2016).

In layer 5 pyramidal neurons, Ca^{2+} fluorescence signals in distal apical trunk dendrites specifically reflect locally generated Ca^{2+} spikes rather than Na^{+} action potentials back-propagating from the axosomatic compartment (Pérez-Garci et al., 2006; Xu et al., 2012a; Harnett et al., 2013; Beaulieu-Laroche et al., 2019). Thus, we measured dendritic spikes in auditory corticofugal neurons using 2-photon imaging of apical trunk dendrites 150-300 µm below the pial surface (Figure 1F). We quantified the activity of 1554 apical trunks in 78 sessions from 14 mice engaged in the GO/NO-GO task.

GCaMP6f signals in dendritic regions of interests (ROIs) were of large amplitude and displayed fast kinetics (Figure 1G. Median half-width and amplitude: 183 ms and 3.7 ΔF/F). These results are similar to previous reports of GCaMP6f signals from layer 5 trunk dendrites in somatosensory cortex (Ranganathan et al., 2018), implying that auditory corticofugal GCaMP6f signals are mediated by similar mechanisms. 56.7% (n=880) of dendrites showed task-related modulation during task performance, defined as a statistically significant change in Ca^{2+} event rate during the sound or answer period on correctly answered GO and/or NO-GO trials.

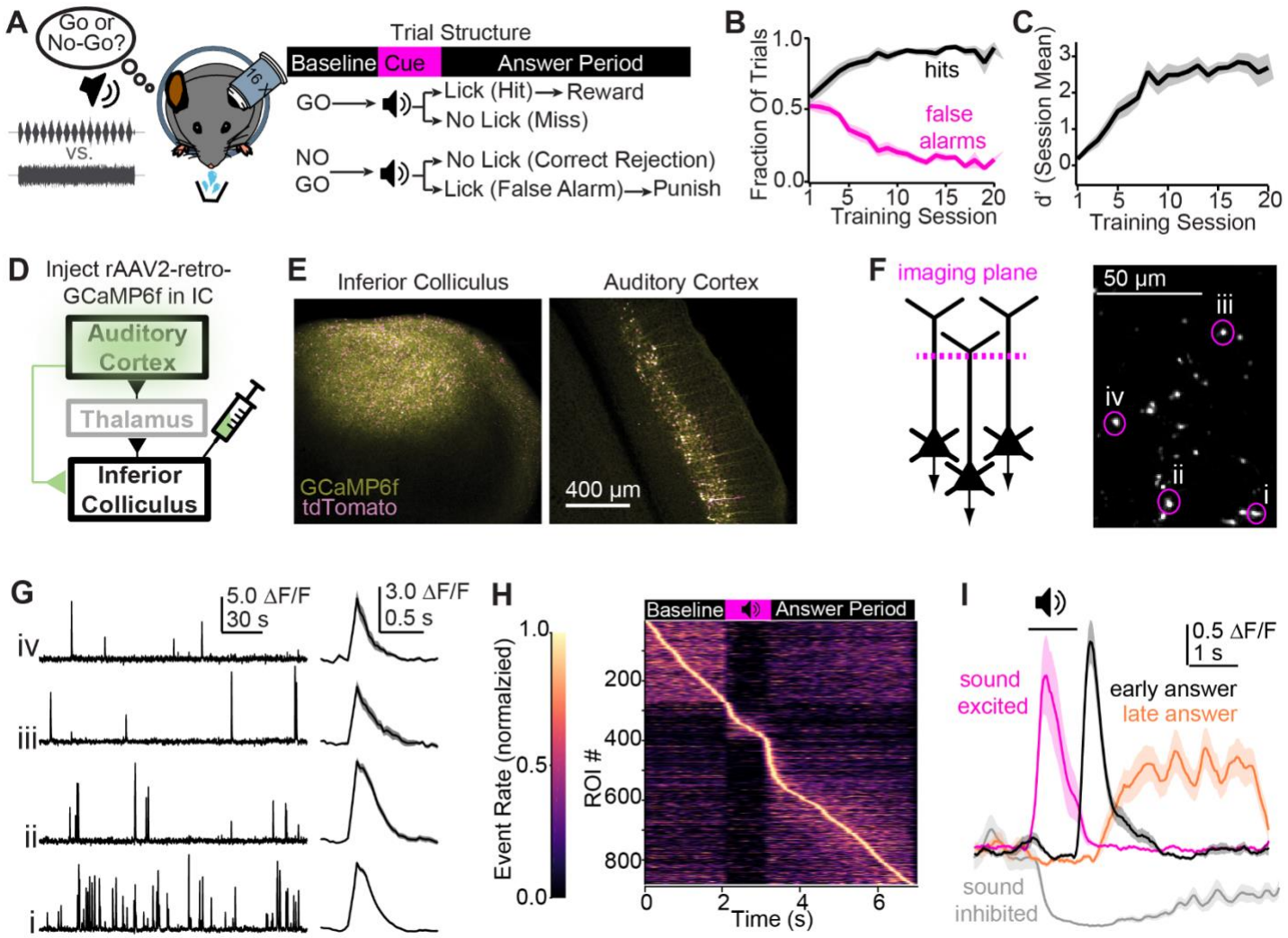

Figure 1: *Dendritic Ca^{2+} spikes in auditory corticofugal neurons of behaving mice.* **A)** Cartoon and trial structure. **B)** Mean hit (black) and false alarm (magenta) rates across learning for n = 14 mice. **C)** Similar to panel B, but for the sensitivity index (d-prime). **D)** A retrograde GCaMP6f virus injected in the IC labels corticofugal neurons. **E)** Confocal micrographs of the IC (Left) and auditory cortex (Right) show preferential retrograde labeling of layer 5 pyramidal neurons. **F)** Trunk dendrites are imaged ~150-300 µm below the auditory cortical surface. Micrograph (right) is an example FOV with dendrite cross-sections visible as circular or ovoid structures; i-iv denote example ROIs. **G)** Fluorescence time series from ROIs in panel F. Dendritic spikes are observable as large and fast transients. Right: Mean Ca^{2+} spikes in each ROI after onset alignment of individual transients. **H)** Normalized event rates of n = 880 task modulated dendrites. Of note is the paucity of dendrites with peak rates during sound presentation. **I)** Example averages for distinct type task-modulated dendrites. Shading in all panels is ±SEM.

Interestingly, only 11.9% (n = 105) of task-modulated dendrites showed activity increases during the sound cue (Figure 1H; Figure 1I, magenta). Instead, 48% (n=425) of dendrites showed a significant *reduction* in Ca^{2+} events during the sound, thereby reducing the mean fluorescence relative to baseline (Figure 1I, grey). These data suggest that auditory activity generates powerful dendritic inhibition onto auditory corticofugal neurons. In addition, 45% of dendrites (n=398) were active in the answer period either during the first second following sound offset (early answer responses; n = 98; Figure 1I, black), for several seconds during the inter-trial interval (late answer responses; n = 185; Figure 1I, orange), or during both early and late answer epochs (n = 115). During active listening, dendritic spikes in auditory corticofugal neurons are for the most part surprisingly anti-correlated with behaviorally relevant sounds. Moreover, only 34% of sound excited (n = 36/105) and 18% of sound inhibited dendrites (n = 78/425) significantly increased their activity during the answer period, implying that the different activity patterns of corticofugal neurons in our task reflect largely non-overlapping populations.

Sound and answer responsive dendrites are preferentially active on GO trials

The distinct activity profiles of corticofugal neurons may reflect preferential responses on GO or NO-GO trials (O'Connor et al., 2010). We tested if activity was differentially modulated during the sound and answer period of GO and NO-GO trials by calculating a selectivity index for each task-modulated dendrite. Values of +1 and -1 indicate that dendritic spiking is exclusively modulated on GO and NO-GO trials, whereas a value of 0 indicates identical modulation on each trial-type. The population distribution of selectivity indices in sound excited dendrites was positively skewed, e.g. showed a strong bias towards GO trials (Figure 2A; median selectivity index = 0.56). This result was not due to an innate preference of dendritic spikes for particular acoustic features, as the distribution of selectivity indices was similar across mice trained with the sAM sound as the GO and NO-GO stimuli (p=0.998, Kolmogorov-Smirnov test). Importantly, Ca^{2+} spikes in GO selective, sound excited dendrites generally occurred prior to mice's first lick on GO trials (Supplemental Figure 1A; median Δ time relative to first lick: -0.34 s, n=79 dendrites, p<0.0001 compared to hypothetical 0 median distribution, signed-rank test), indicating that neural activity in these dendrites was likely driven by sound rather than motor activity. Conversely, selectivity indices of sound inhibited dendrites centered near 0 (median = 0.0253, Figure 2B), reflecting a powerful and non-specific reduction of dendritic spikes during the sound. In addition, many sound inhibited dendrites also displayed sustained inhibition during the answer period on GO trials (Figure 2B), implying that this dendritic inhibition is activated by sound and motor signals. Both early and late answer responsive dendrites had positively skewed selectivity indices similar to sound excited dendrites (Figures 2C,D. Median values of 0.61 and 0.85, respectively), indicating that answer period activity occurs primarily (though not exclusively) on GO trials. However, in contrast to sound excited dendrites, GO selective answer responsive dendrites increased their activity *after* mice began licking the water spout for rewards (Supplemental Figure 1B,C; median Δ time relative to first lick: +1.48 s, n = 320 dendrites, p<0.0001 vs. a hypothetical 0 median distribution, signed-rank test). These data show that dendritic spikes preferentially occur on trials involving reward predictive sounds and reward-related licking. Answer responses may thus reflect motor activity, rewards, or alternatively, responses biased to the termination of reward predictive sounds (Lee and Rothschild, 2021).

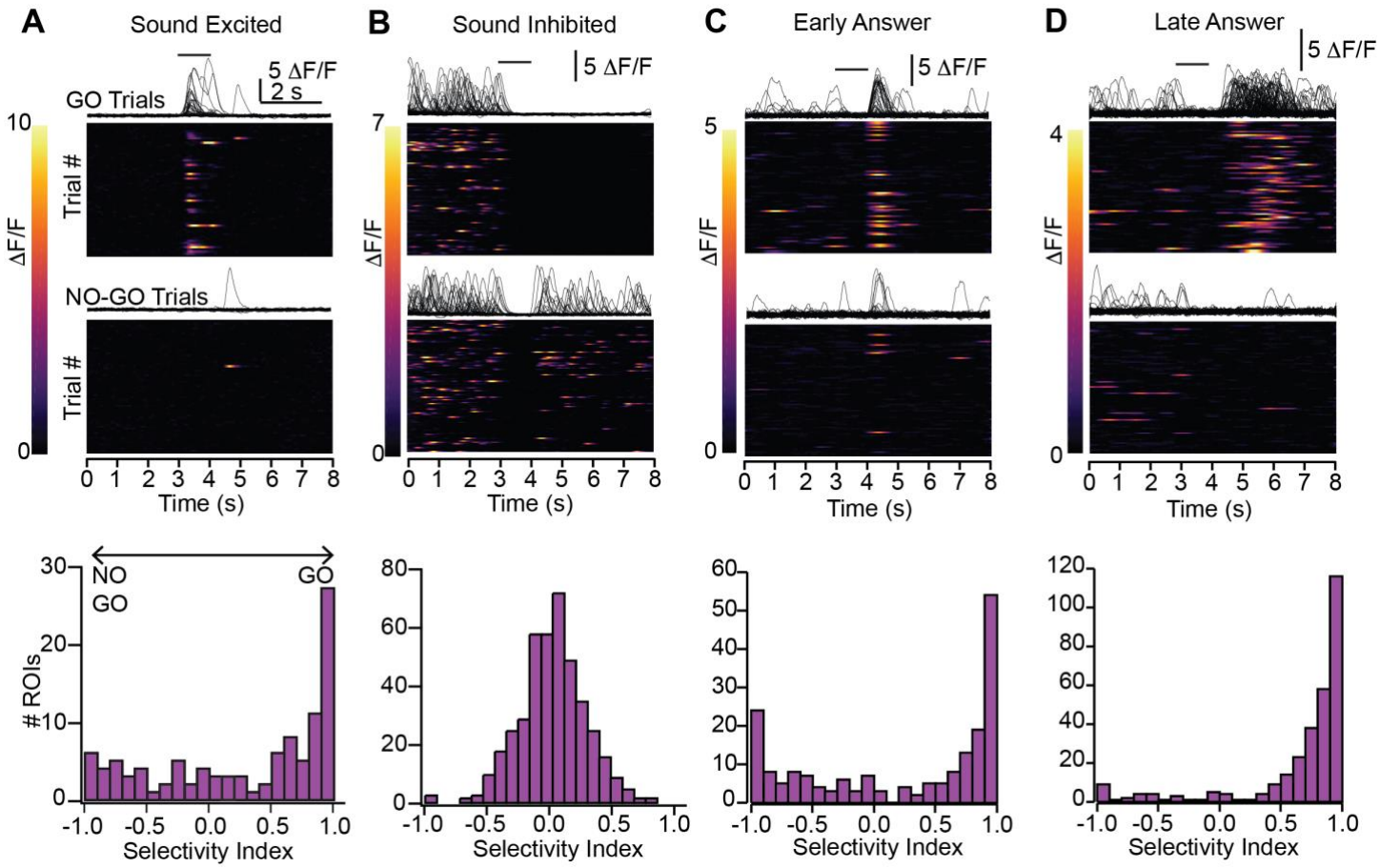

Figure 2: *Dendritic spikes are biased towards GO trials.* **A)** Example heatmaps from correctly answered GO and NO-GO trials in a sound-excited dendrite are shown in the upper panels, with corresponding raw traces. Black bar denotes sound onset The lower panel histogram shows the distribution of selectivity indices (see Results and Methods) across the population of sound excited dendrites. B-D are organized same as panel A, but for sound inhibited (**B**), early answer (**C**) and late answer dendrites (**D**).

Answer selectivity on GO trials reflects goal-directed licking, independent of reward consumption

The biased selectivity of dendritic spikes during the answer period of GO trials could encode the termination of a behaviorally relevant sound features. Indeed, the temporal precision of early answer responses (Figure 2C) is reminiscent of auditory cortical “OFF” responses (Liu et al., 2019; Solyga and Barkat, 2021) that are known to be patterned by the learned salience of sounds (Lee and Rothschild, 2021). If this hypothesis is correct, GO selective dendrites should have distinct activity profiles on GO and NO-GO trials where different sound cues are presented, regardless of mice’s behavioral choice during the answer period (Figure 3A, left). Alternatively, answer period activity could reflect movement signals (e.g., licking) during reward consumption (Huang et al., 2019; Lacefield et al., 2019). In this case answer period activity should be similar on hit and false alarm trials; mice would hear different sounds but perform similar operant actions (Figure 3A, right). Most GO selective, answer responsive dendrites were active on both hit and false alarm trials and showed far less activity on correct rejection trials; this result held true across early and late answer populations (Figure 3B,C). Additionally, there was a significant positive correlation between dendritic spike probability on hit and false alarm trials (Figure 3D; Pearson’s rho =0.62, $p<0.001$). Thus, dendritic spikes during the answer period of GO trials reflect mice’s instrumental actions rather than sound termination.

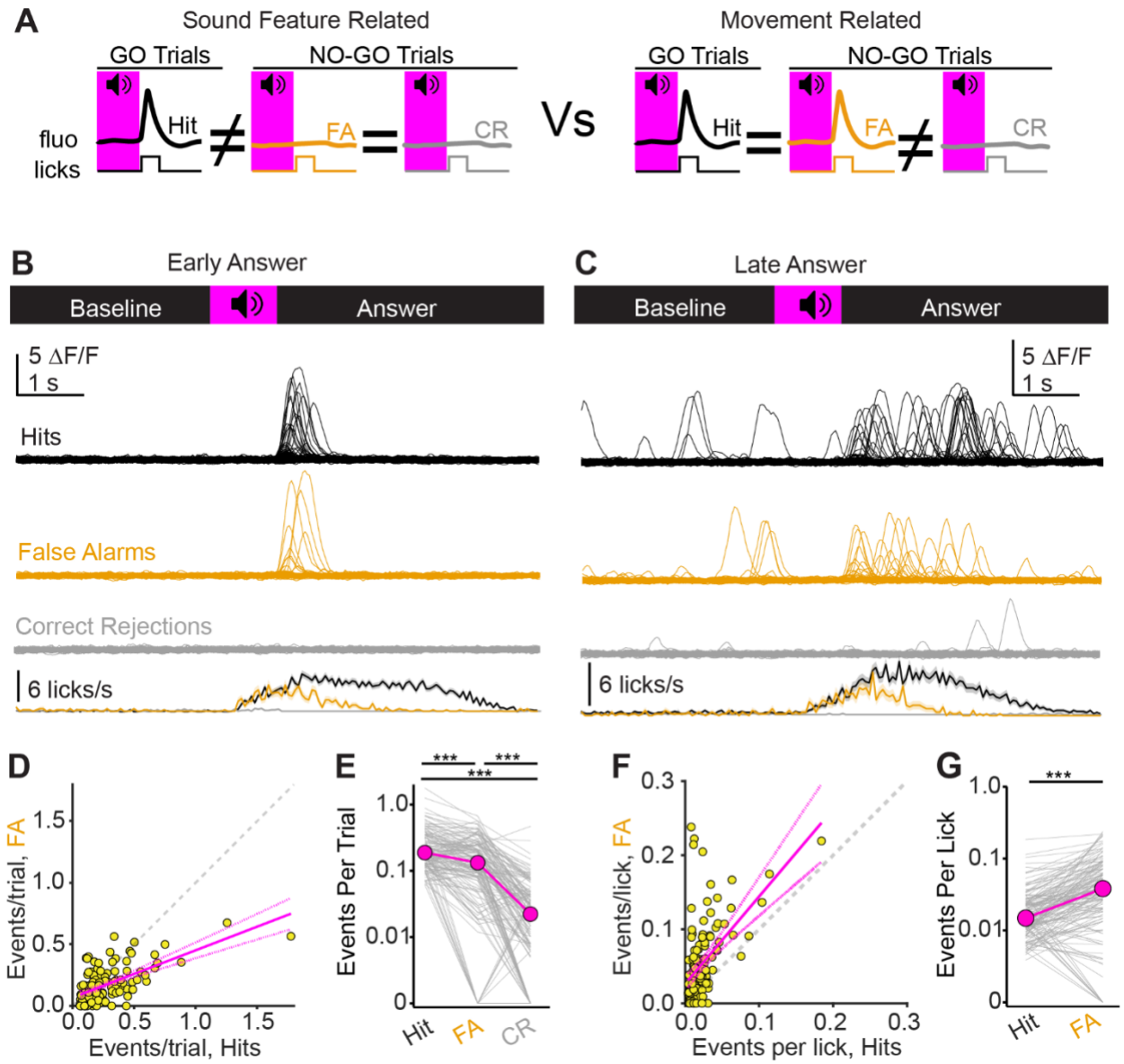

Figure 3: *GO-selectivity in answer responsive dendrites reflects goal-directed licking.* **A)** Cartoon of analytical rationale. **B)** Example traces and lick rate histograms (upper and lower panels, respectively) from an early answer responsive dendrite. Of note are dendritic spikes occurring on hits and false alarms, but not on correct rejections. **C)** Same as panel B, but for a late answer responsive dendrite. **D)** The number of dendritic spikes per trial on false alarms versus hits (y and x axes, respectively) for answer responsive dendrites. Magenta is the linear fit with 95% confidence intervals. The gray dotted line is the unity. **E)** Events per trial across the three trial outcome conditions for answer responsive dendrites. Gray lines are individual ROIs, magenta is median. **F)** Same as D, but normalized to the number of licks on each trial. Most points fall above the unity line, indicating more dendritic spikes per lick on false alarms compared to hits. **G)** Events per lick on hits and false alarms. Asterisks denote statistical significance. Of note, y-axes for E and G are on a log scale. Early and late dendrites are pooled in all analyses.

Indeed, dendritic spike probability was generally higher on hit compared to false alarm trials (Figure 3E. Median event probability per trial: 18.8, 13.2 and 2.2% for hits, false alarms, and correct rejections, respectively. $F(3,137)=176.8$, $p<0.0001$, Friedman test. $P<0.0001$ for all pair-wise comparisons, Dunn's post-hoc tests). However, this result likely reflects differences in the absolute number of licks mice

made on each trial type: Normalizing the dendritic spike probability to mice's lick rate revealed a *greater* probability of dendritic spikes on false alarm compared to hit trials (Figure 3F,G. Median events per lick: 0.015 vs. 0.038 for hit and false alarm trials, respectively. $p<0.0001$, signed-rank test). The data suggest either a ceiling effect for dendritic spikes triggered by licking bouts, or alternatively, that reward consumption has a net inhibitory effect on dendritic electrogenesis. Furthermore, the peak fluorescence of individual dendritic events was similar on hits and false alarm trials, implying that mice's actions control the probability, but not the magnitude of dendritic spikes (Median peak $\Delta F/F$ of 3.37 vs. 3.47 for hits and false alarms, respectively. $p=0.58$, signed-rank test). *In tandem* with the results of Figure 2, our data imply that the biased selectivity of dendritic spikes towards GO trials reflects two mechanisms: In sound excited dendrites, a learning-dependent process biases dendritic responses towards behaviorally relevant sound features, whereas answer period activity is yoked to the initiation and continued execution of goal-directed movements, a process which may or may not be patterned by learning. Finally, although answer period activity was largely skewed towards GO trials, a small population of dendrites responded preferentially in the answer period of correctly answered NO-GO trials and also correlated with mice's choice (Supplemental Figure 2. See also Figure 2C,D): Activity preferentially occurred on correct rejection trials and was less likely prevalent on false alarm trials. One potential interpretation is that this NO-GO selectivity reflects high-level signals related to the withholding of licking. Alternatively, these dendrites may be broadly tuned to sound termination, and the lack of activity on false alarm trials could reflect licking-related inhibition.

Silencing answer period activity impairs discriminative learning

Corticofugal neurons are important for many learned and innate behaviors (Bajo et al., 2010; Znamenskiy and Zador, 2013; Liu et al., 2016; Ruediger and Scanziani, 2020; Tang and Higley, 2020), and dendritic spikes could be potential effectors of synaptic plasticity to support these processes (Ranganathan et al., 2018). We find that a major fraction of dendritic spikes reflects motor activity *after* the discriminative sound has ended. Does this answer period activity contribute to the learning-related functions of corticofugal neurons? If it does, selective silencing of auditory corticofugal neurons *after* sound presentation should suffice to impair learning. To this end, we bilaterally expressed the inhibitory opsin GtACR1 in auditory corticofugal neurons by injecting a retrograde-cre recombinase virus in the IC of GtACR1 fl/fl mice (Li et al., 2019). Patch-clamp recordings confirmed that GtACR1 activation potently dampened auditory corticofugal activity, such that 625 nm light at >3 mW largely abolished spiking even to >1 nA current steps (Supplemental Figure 3). We next tested if silencing answer period activity impacts mice's learning of the GO/NO-GO sAM task by comparing the learning rates of GtACR1 fl/fl mice injected with a retrograde-cre virus or control saline buffer (Figure 4A,B). Mice were trained using a standardized protocol, in which auditory corticofugal neurons were silenced bilaterally via light delivered to the auditory cortex *only* during the answer period on each trial (Figure 4C). Because GtACR1 is not activated during the sound presentation, any effect on learning should be independent of a corticofugal contribution to sound perception or discrimination. Mice were first trained to associate a GO sound with reward availability, and upon reaching criterion (>75% hits on two consecutive sessions), trained to discriminate GO and NO-GO sounds presented with 50% probability (Figure 4D).

Both mouse groups showed similar increases in hit rates when exposed only to GO cues (Figure 4E. Median number of sessions to criterion: 4 and 5 for control and GtACR1 mice, respectively. $p=0.89$, Kolmogorov-Smirnov test). Thus, silencing answer period activity does not appear to impair mice's motivation or ability to learn simple, operant associations. By contrast, GtACR1-expressing mice showed a significant reduction in d-prime across GO/NO-GO training sessions compared to control mice (Figure 4F; mixed effects model. Main effects of session and treatment group: $F(1,28)=5.479$,

p=0.027 and F(6.44,178.1)=63.42, p<0.0001, respectively), and the maximum d-prime reached across all sessions was significantly lower for GtACR1 compared to control mice (Figure 4G; 3.3 ± 0.2 vs 2.6 ± 0.2 for n = 15 control and n = 15 GtACR1 expressing mice, p=0.010, unpaired t-test). Consequently, the cumulative distribution of d-prime values in sessions 11-15, during which mice's discrimination has typically reached a plateau (Figure 1C,7F), was left-shifted in GtACR1 relative to control mice (Figure 4H; p=0.002, Kolmogorov-Smirnov test). These group-level differences do not reflect impaired learning from cre recombinase or GtACR1 expression in corticofugal neurons, as a separate cohort of n = 11 control and n = 12 GtACR1-expressing mice trained in absence of LED activation showed similar sensitivity indices across sessions (Mixed-effects model. Main effect of Session #: F(4.553, 95.61)=22.46, p<0.001; No effect of treatment group: F(1,21)=0.8053, p=0.38). Rather, the results reveal an unexpected non-sensory component to corticofugal neuron function.

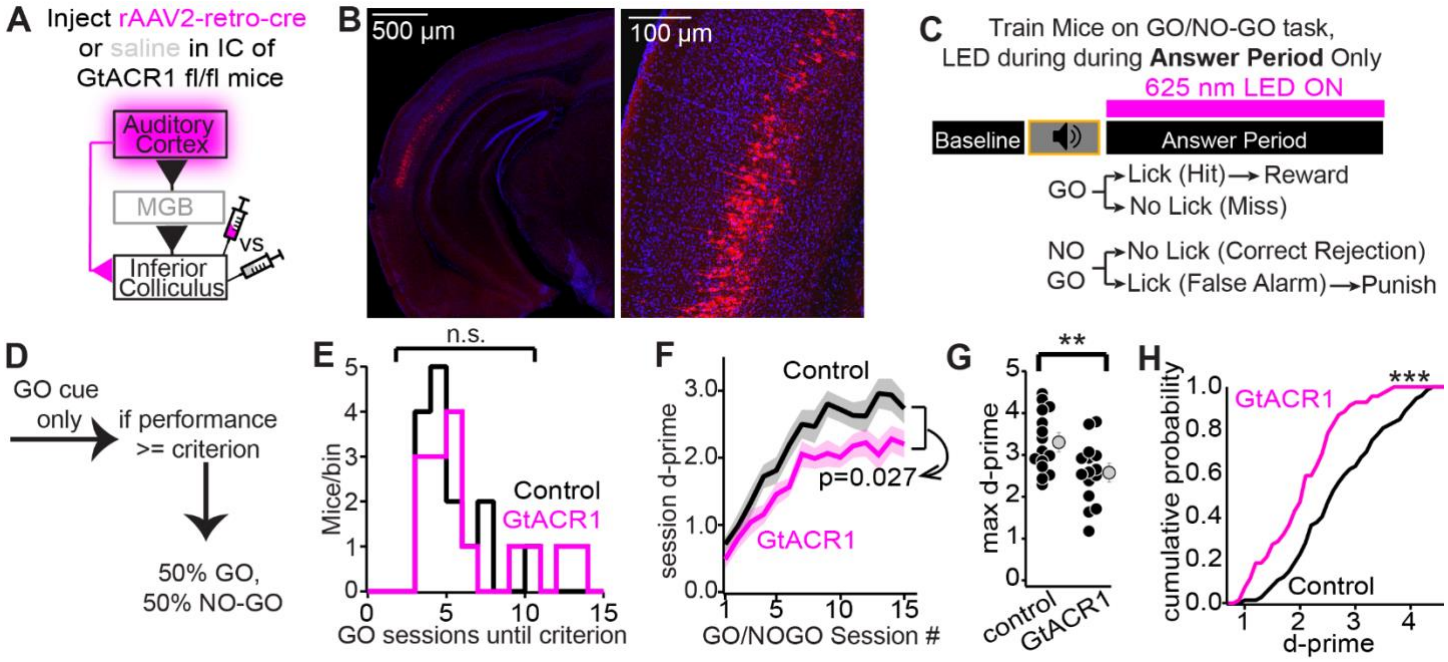

Figure 4: *Answer period activity contributes to discriminative learning*. **A)** A retrograde-cre virus or control buffer is injected bilaterally in the IC of GtACR1 fl/fl mice. **B)** Micrographs of GtACR1 expression in layer 5 corticofugal neurons of auditory cortex. The FusionRed tag, and thus GtACR1 construct, is soma-targeted in these mice (Li et al., 2019). **C)** Mice are trained on the GO/NO-GO discrimination task. Bilateral LEDs over auditory cortices are activated on all trials *only* during the answer period. **D)** Mice are initially trained to associate the GO sound with rewards, and upon reaching criterion, are trained on the full GO/NO-GO task. **E)** Histograms of the number of GO-only sessions until criterion for control (black) and GtACR1 mice (magenta) **F)** Mice's d-prime across GO/NO-GO training sessions. Lines + shading are mean ± SEM of each group **G)** Maximum d-prime across sessions 11-15 for both groups of mice. Black dots are individual mice, grey is mean ± SEM. **H)** Cumulative distribution of d-prime values in sessions 11-15 for control and GtACR1 expressing mice. Asterisks denote statistical significance.

Discussion

By switching neuronal spiking from low-frequency trains to high-frequency bursts, dendritic Ca^{2+} spikes trigger a uniquely strong output signal (Xu et al., 2012a; Takahashi et al., 2016, 2020; Ranganathan et al., 2018; Beaulieu-Laroche et al., 2019; Francioni et al., 2019; Trautmann et al., 2021) that may signal correlated activity in basal and apical dendrites receiving largely distinct pre-synaptic inputs (Larkum et al., 1999, 2022; Takahashi and Magee, 2009; Bittner et al., 2015). We show that in auditory corticofugal neurons of behaving mice, the majority of dendritic spikes occurred *after* the discriminative sound

stimulus and were driven by mice's purposeful actions. Although little is known regarding the specific synaptic inputs that drive motor-related dendritic spikes, the responsible pathways may arise from sub- or intra-cortical regions (Schneider et al., 2014; Nelson and Mooney, 2016; Clayton et al., 2021) and could transmit motor efference copies, proprioceptive signals, or potentially, a learned representation of rewarded actions (Peters et al., 2017; Park et al., 2022). Regardless of the precise mechanism, we show that silencing such motor activity in auditory corticofugal neurons impairs discriminative learning, thereby highlighting a novel function for the movement related signals observed throughout sensory cortices (Musall et al., 2019; Stringer et al., 2019).

Our data further dovetail with several studies intimating a learning-related role for layer 5 neurons of sensory cortex (Xiong et al., 2015; Ranganathan et al., 2018; Ruediger and Scanziani, 2020). Indeed, chemical ablation of the auditory cortico-collicular neurons studied here prevents relearning of sound localization following monaural hearing loss (Bajo et al., 2010). A tacit assumption is that these learning impairments perhaps reflect a loss of sensory-evoked signals from the neo-cortex, which could support learning by increasing sensory discrimination (Znamenskiy and Zador, 2013). However, our data imply that these findings may also stem from a loss of descending motor signals transmitted several seconds after a discriminative stimulus has subsided. Consequently, the results agree with data from motor, visual and somatosensory cortices indicating that "trial outcome" or "action timing" activity contributes to the acquisition of sensorimotor behaviors (Namboodiri et al., 2015; Levy et al., 2020; Schoenfeld et al., 2021).

Dendritic Ca^{2+} spikes as cell-intrinsic and efferent effectors of supervised plasticity

How might motor-related activity support learning? In hippocampus CA1 neurons, dendritic Ca^{2+} spikes can potentiate excitatory synapses active even >1 s prior to a dendritic spike (Bittner et al., 2017), thereby instructing plasticity at synapses whose activity precedes, but does not directly initiate dendritic electrogenesis. Thus, dendritic spikes in pyramidal neurons may act as a cellular correlate of model-free "supervised" learning algorithms (Sutton and Barto, 2018), similar to the hypothesized function of dendritic Ca^{2+} spikes in the Purkinje and Purkinje-like cells of mammalian cerebellum and mormyrid fish's electrosensory lobe (Bell et al., 2008; Raymond and Medina, 2018). If a similar plasticity rule exists in layer 5 pyramidal neurons, motor-related dendritic spikes could promote heterosynaptic potentiation of "bottom-up" synapses transmitting information regarding the discriminative sound cues; such a plasticity rule could enhance the representation of behaviorally relevant GO sounds. Accordingly, many sound-responsive dendrites in our dataset were biased towards reward-predictive sounds. Given that dendritic Ca^{2+} fluorescence in layer 5 neurons exclusively indexes burst firing (Xu et al., 2012a; Beaulieu-Laroche et al., 2019), this dendritic activity may be the "tip of the iceberg" for a dense over-representation of reward-related sound information transmitted via lower-frequency spike trains. Consequently, such a plasticity rule might partially explain classic findings of sound feature over-representation in auditory cortex during development (Zhang et al., 2001), Pavlovian conditioning (Edeline et al., 1993), and instrumental learning (Polley et al., 2006; Bieszczad and Weinberger, 2010).

Alternatively, the action potential bursts triggered by dendritic spikes may function as instructive or permissive forces for plasticity in target brain regions. In agreement, auditory corticofugal neurons are required for re-learning of a sound localization task upon hearing loss (Bajo et al., 2010), but the auditory cortex is apparently dispensable for task performance after animals have re-learned to localize sounds with altered cues (Bajo et al., 2019). Thus the plasticity mechanisms recruited during learning may instead reside in postsynaptic targets of corticofugal neurons. Intriguingly, neural network models which implement dendritic spike-mediated burst firing can solve the "credit assignment problem" without

resorting to biologically inaccurate back-propagation algorithms (Payeur et al., 2021). Although the precise degree of similarity between corticofugal pathways and artificial neural networks remains equivocal, it is nevertheless conceivable that spike bursts from high-level brain regions propagate an instructive signal to hierarchically lower levels of the network, e.g. neurons in the IC. In support of this hypothesis, classic studies show that auditory cortex orchestrates rapid receptive field plasticity of IC neurons (Yan and Suga, 1998; Suga et al., 2002; Ji et al., 2005), whereas data from avian show that IC neurons are major loci of learning- and NMDA receptor-dependent plasticity (Brainard and Knudsen, 1993; Feldman et al., 1996; Penzo and Peña, 2009). Interestingly, recent *in vitro* data show that auditory corticofugal activity promotes cooperative NMDA receptor activation at ascending synapses in IC neurons (Oberle et al., 2022). If IC neurons are capable of long timescale learning rules similar to hippocampus neurons, motor-related activity in corticofugal neurons might support learning by instructing heterosynaptic plasticity at “bottom-up" synapses onto neurons of evolutionarily ancient brain regions.

Methods

Surgeries

All surgical procedures were approved by the University of Michigan’s IACUC, performed in accordance with NIH’s guide for the care and use of laboratory animals, and conducted under aseptic conditions. For imaging experiments, C57BL6/J mice (5-7 weeks of age; Jackson stock #000664) were deeply anesthetized with 4-5% isoflurane vaporized in O^2 and mounted in a rotating stereotax (David Kopf Instruments). Isoflurane was subsequently lowered to 1-2% to maintain a stable anesthetic plane, as assessed by the absence of paw withdrawal reflex and stable respiration (1-1.5 breaths/s). Body temperature was maintained near 37-38 C using a feedback controlled, homeothermic heating blanket (Harvard Apparatus). Mice were administered carprofen (5 mg/kg, s.c.) as a pre-surgical analgesic, the fur and skin overlaying the skull was removed and 2% topical lidocaine was applied to the wound margins. The dorsal portion of the skull was cleaned and scored in a checkerboard pattern using a scalpel. A 300-500 µm craniotomy was carefully drilled over the left IC (0.9 mm caudal and 1.0 mm lateral from the lamboid sutures) using a 0.5 mm dental burr and microdrill (Foredom). The skull was frequently irrigated with chilled PBS to prevent heating, and care was taken as to not rupture the transverse sinus or overlaying dura mater during drilling. Following the craniotomy, a glass pipette (tip diameter: ~100 µm) containing the retrograde AAV-hSyn1-GCaMP6f-P2A-nls-dTomato virus (Addgene #51085) was slowly lowered into the IC at a rate of 1 µm/s using a micromanipulator (Sutter MP-285). A total of 125-165 nL was injected at 5 different sites in the IC (25-33 nL/site, 1 nL/s) per mouse. Following injections, the pipette was maintained in place for an additional 3-5 min before retraction at a rate of 10 µm/s. The craniotomy over the IC was then filled with bone wax and the dorsal surface of the skull was covered with a thin layer of cyanoacrylate glue. Subsequently, the left temporal muscle was retracted and the stereotax was rotated ~50 degrees, thereby enabling a vertical approach to the lateral left portion of the mouse’s skull. A ~2 mm diameter craniotomy was carefully opened over the left auditory cortex (2.75 mm caudal from bregma centered over the lateral ridge). The dura overlying the auditory cortex was left intact, and a custom cranial window (two 2 mm diameter coverslips stacked upon one another and affixed to a 4 mm outer coverslip with UV-cured Norland Adhesive #71) was gently implanted over the exposed brain. The coverslip was affixed to the skull using cyanoacrylate glue and reinforced with dental cement (Lang dental). Following cranial window implantation, the rotating stereotax was repositioned horizontally and a lightweight titanium headbar was affixed to the mouse’s skull using dental cement. The mouse was then removed from the stereotax, administered a post-operative analgesic (buprenorphine, 0.03 mg/kg) and allowed to recover from surgery in a clean

home cage on a heating pad. Mice were then returned to the vivarium. Supplemental doses of carprofen were administered 24 and 48 hours following surgery.

For behavior and optogenetic experiments of Figure 4, surgeries were conducted as described above, except that a retrograde-cre virus (pENN.AAV.hSyn.Cre.WPRE.hGH; Addgene #105553) or sterile PBS was injected bilaterally in the IC of 6-8 week old GtACR1 fl/fl mice (Jackson stock # 033089) and 4 mm diameter coverslips were implanted over the thinned skull of both auditory cortices. 4-5 week old GtACR1 mice were used for the experiments of Supplemental Figure 3. Here, an incision was gently made in the skin overlying the skull, a hole was drilled over the left IC to unilaterally inject ~100 nL of retrograde-cre virus. Following injections, the pipette was retracted, the skin was sutured and post-operative care was provided as described above.

Behavior during 2-photon Ca^{2+} Imaging

Mice were single housed under a reversed light/dark cycle (12/12 hr). Food, and initially water, were provided ad libitum. 3-7 days following surgery, mice's water ration was restricted to 0.5-1.5 mL water/day, depending on weight loss and motivation. Body weight was monitored daily and kept above 70 % of the ad libitum weight. Following 5-7 days of water restriction, mice were handled by an experimenter and habituated to head-fixation while sitting in a Plexiglas tube, similar to the protocol described by Guo and colleagues (2014). After one to two initial habituation sessions of ~30 min each, mice were trained on the auditory GO/NO-GO discrimination task once per day in custom-made sound-attenuating booths. The behavioral protocol was controlled by BPod hardware and related Matlab code (Sanworks). During behavioral sessions, an optical lickport (Sanworks) connected to a reward spout was placed within 1-2 cm from the mouse's mouth. On each trial, a 1-s sound (band-passed white noise, 4-16 kHz bandwidth; 0 or 100% 15 Hz modulation depth, calibrated to 70 dB with a ¼" microphone (Bruel & Kjaer) was presented through a speaker (Peerless XT25SC90-04) located horizontally ~10 cm away from the mouse's right ear. Stimulus category (GO or NO-GO) was pseudo randomly assigned as 0 or 100 % sAM depth for each animal. On GO trials, licking the reward spout during a 1.5 s "answer period" following sound termination resulted in the opening of a solenoid valve (located outside of the sound attenuating chamber) and delivery of a ~ 2 µL drop of 10% sucrose water. On NO-GO trials, licking the water spout during the answer period resulted in a "time-out", where the inter-trial interval increased by 5-10 s. Licking the water spout at any other time during the trial had no effect, and consequently mice learned to lick mainly during the answer period on GO trials after 5-10 training sessions. Behavioral sessions consisted of approximately equal numbers of randomly presented GO and NO-GO trials, with no more than three consecutive trials being of the same trial type. Sessions typically lasted 1.5-3 hours, during which time mice performed ~250-600 trials.

Imaging data acquisition typically commenced once mice performed at a global average of 75-80% correct for a minimum of two consecutive training sessions. Mice underwent a maximum of 5 imaging sessions/week (maximum one per day, Monday-Friday) for 2 to 5 weeks following surgery. At the beginning of each imaging session, a temporary silicone well was built around the cranial window to hold saline solution. Experiments were performed using a resonant-galvo 2-photon microscope similar to the Janelia MIMMs design (Sutter Instruments) and a water immersion 16x objective (Nikon). The microscope was housed in a custom sound-attenuating chamber. The microscope objective was rotated 40-50 degrees to be approximately orthogonal to the cranial window over auditory cortex. GCaMP6f was excited with a Titanium-Sapphire laser at 920 nm (Coherent Chameleon Ultra II). During each session, we imaged a single field of view (~350 μm^2) 150-300 µm below the pial surface containing apical trunk and/or tuft dendrites of layer 5 cortico-collicular pyramidal neurons. Typically,

data could be acquired from 2 to 8 non-overlapping fields of view per mouse. On each trial, 7-8 s of imaging data were acquired with Scanimage software at 30 Hz, with a minimum trial-to-trial interval of 8 s. Behavior data were acquired simultaneously and synchronized with imaging data offline. At the end of each session, the silicone well was removed and mice were returned to their home cage. Mice's water intake was estimated by calculating the difference in body weight (including droppings) before and after each behavior session. Mice were provided with additional water (0% sucrose) in their home cage if they did not receive their full daily water ration during the sessions. Similarly, mice were provided with appropriate rations of 0% sucrose water on days in which they did not participate in behavioral experiments.

Behavior during optogenetic manipulations

Surgeons and experimenters were blinded to mice's treatment condition throughout the course of these experiments. Following a week of recovery from surgery, mice were placed on water restriction and handled by the experimenter for 7 days prior to training. Three days prior to training, all mice were habituated to head fixation for sessions of up to 30 min over a three day period. All mice followed a standardized training protocol whereby head-fixed mice were first trained on 250 trials/day to lick a water-spout within 2 s following a GO cue to receive a drop of sugar water reward (band-pass white noise, 4-16 kHz, 1 s duration, 75-82 dB SPL for all mice). Upon reaching criterion of >75% hits/session for 2 consecutive sessions, the NO-GO cue (4-16 kHz band-pass white noise with 15 Hz modulation rate, 75-82 dB SPL) was introduced in the following session and false alarms were punished with a 7 s timeout as described above. In the first session following criterion, mice initially received 100 sequential GO trials, followed by a total of 200 interleaved GO and NO-GO trials (50% NO-GO probability). This initial "transition session" was discarded from analyses. All subsequent sessions contained 300 pseudo-randomly interleaved GO and NO-GO trials (50% NO-GO probability), with no more than 3 sequential repetitions of the same trial type. Auditory corticofugal neurons were silenced for 2 s during the answer period via 625 nm LED coupled optic fibers (400 µm diameter, 0.5 NA) positioned atop cranial windows overlaying the auditory cortices. LED power at the fiber tip was 10-12 mW. We estimated the power loss through the skull and brain to be ~1 mW. To this end, we compared the power output of the 625 nm LED, before and after placing a mouse parietal skull plate lined with ~1 mm thick 2% agarose between the optic fiber and the power meter detector. We used 625 instead of 473 nm light due to the decreased scattering of longer wavelengths in brain tissue. In addition, prior experiments in neo-cortex (Li et al., 2019) and our in vitro calibration data (Supplemental Figure 3) show robust GtACR1 activation at 625 nm.

Imaging data analysis

Movies were registered and motion corrected with the Suite2p package running in Matlab or Python (Pachitariu et al., 2016). ROIs for individual dendrite segments were generated using the Caiman package running in Matlab 2017b (Pnevmatikakis et al., 2016; Lacefield et al., 2019). Fluorescence time series of individual ROIs were generated by averaging the frame-by-frame intensity of pixels corresponding to binary masks of dendrite segments. To convert raw fluorescence to $\Delta F/F$, baseline fluorescence of each ROI was defined as the median pixel intensity over the course of 20-30 trials (160-240 s of data). Spatially non-overlapping ROIs in the same FOV occasionally showed high degrees of temporal correlation, in agreement with previous studies showing that dendritic Ca^{2+} transients in layer 5 pyramidal neurons are often globally synchronized across multiple dendritic branches (Xu et al., 2012a; Ranganathan et al., 2018; Beaulieu-Laroche et al., 2019; Kerlin et al., 2019). We considered highly correlated dendrites (>0.5 cross-correlation coefficient; Ranganathan et al., 2018) as originating from the same neuron, and thus only a single ROI was kept for the analyses

reported here. For each ROI, the timing and peak of Ca^{2+} events were detected using a threshold crossing algorithm after smoothing traces with a 4-point median filter.

In vitro electrophysiology

~2 weeks following surgery, mice were deeply anesthetized with isoflurane, decapitated, and the brains quickly removed in ice cold, oxygenated solution containing (in mM): 87 NaCl, 2.5 KCl, 1.25 NaH_2PO_4, 7 $MgCl_2$, 25 glucose, 75 sucrose, 25 $NaHCO_3$, 1 ascorbate, 1 pyruvate, 0.5 $CaCl_2$. 300 μm thick coronal slices containing the auditory cortex were sectioned with a vibratome (Campden instruments) followed by a 30 min recovery incubation in oxygenated, 34 C artificial cerebro-spinal fluid (ACSF; in mM): 119 NaCl, 25 $NaHCO_3$, 3 KCl, 1.25 NaH_2PO_4, 15 glucose, 1 $MgCl_2$, 1.3 $CaCl_2$, 1 ascorbate, 3 pyruvate. Following recovery, a slice was transferred to a recording chamber under an Olympus BXW51 microscope and continuously perfused with oxygenated 32-34 C ACSF (2-4 mL/min, chamber volume: ~1 mL). Neurons were visualized via Dodt contrast optics using a 63x microscope objective and targeted for patch-clamp recordings based on visually confirmed expression of the FusionRed tag fused to the GtACR1 construct (Li et al., 2019). Current-clamp recordings were obtained with glass pipettes filled with internal solution (in mM): 115 K-gluconate, 4 KCl, 0.1 EGTA, 10 HEPES, 14 Tris-phosphocreatine, 4 Mg-ATP, 0.5 Tris-GTP, 4 NaCl, pH 7.2-7.3, 290 mOsm (open tip resistance: 3-5 MOhm). GtACR1 was activated via a 400 µm diameter optic fiber coupled to a 625 nM LED positioned <1 mm from the recorded cell. Control and LED trials were interleaved during experiments, and we typically recorded 3-4 repetitions of each current step/LED power combination. Data were acquired with an Axon Instruments Multiclamp 700B, low-pass filtered online at 10 kHz, and sampled at 50 kHz with a National instruments PCIe-6343 card and BNC2090A interface controlled by Matlab based Wavesurfer software (Janelia Research Campus). Series resistance (<25 mOhm) was compensated via bridge balance circuitry and pipette capacitance neutralization was employed in all experiments.

Statistics

All statistical routines were run in Matlab, Graphpad Prism 9, or Microsoft Excel. The d-prime was calculated as the difference in z-statistic between hit and false alarm rates across all viable trials in a given session. All analyses were run on task-modulated dendritic ROIs, which were defined as having a Ca^{2+} event probability during the sound and/or answer periods that was significantly different from the baseline period on either GO or NO-GO trials (alpha corrected Wilcoxon signed-rank test). For analyses in Figures 1-3, mice's behavioral performance was >70% (mean d-prime = 2.72 +/- 0.08) and only correctly answered trials were analyzed. In Figure 2, the Selectivity Index for each dendrite was calculated as

$$\frac{\boldsymbol{prob(Event)_{GO} - prob(Event)_{NOGO}}}{\boldsymbol{prob(Event)_{GO} + prob(Event)_{NOGO}}}$$

Analyses in Figure 3 were run on a subset of sessions where mice performed above chance but made enough false alarms on NO-GO trials for meaningful comparisons. We did not include activity on miss trials in these analyses as mice typically had few, if any misses on GO trials during task engagement.

For analyses of behavior data in Figure 4, trials were discarded for d-prime calculations after mice made 5 or more consecutive misses on GO trials, as mice were assumed to be satiated and no longer motivated to perform the task. Both groups of mice performed a similar number of trials until satiety (mean: 284.4 ± 2.9 vs 277.1 ± 3.6; median: 300 vs 300 trials for control and virus groups, respectively. p=0.56, Kolmogorov-Smirnov test).

Although not explicitly determined *a priori*, the sample sizes employed in this work are consistent with established standards in the field. For all within- and between-group comparisons, data were tested for normality using Lilliefors test prior to significance testing. Normally distributed data were compared via parametric tests, whereas non-parametric approaches were employed when one or more of the datasets deviated from normality. Mean ± SEM and median are reported for normally and non-normally distributed data, respectively. Alpha value (<0.05) is corrected for multiple comparisons when appropriate.

Histology and confocal imaging

Mice were euthanized via an overdose of isoflurane within an induction chamber. Transcardial perfusions were performed after breathing and reflexes were absent using PBS followed by 10% buffered formalin. Brains were carefully removed and stored in the dark in 10% formalin overnight at 4°C for immersion fixation. Prior to vibratome slicing, brains were rinsed 3 times over 5 minutes in PBS on a platform shaker and embedded into 4% agar (PBS). Coronal slices (100 µm) were cut using a Leica vibratome (VT1000S) and chilled PBS. Slices containing the IC and auditory cortices were mounted on object slides and covered using Fluoromount-G (SouthernBiotech). Slides were dried at room temperature overnight, sealed using clear nail polish and stored in the dark at 4°C until confocal imaging. Images were collected using a Leica TCS SP8 laser scanning confocal microscope equipped with a 10x objective.

Author Contributions: ANF, JEC, MMR, and PFA collected the data. PFA and MMR analyzed the data. GLQ contributed software and methodology. PFA wrote the paper with contributions from all authors.

Acknowledgements: We thank Drs. Kevin Bender, Travis Moschak, and Gideon Rothschild for thoughtful comments on the manuscript, and Mr. Deepak Dileepkumar for constructing the sound-attenuating chambers + optogenetic LEDs used in these experiments. Funding was generously provided by the Hearing Health Foundation, the Whitehall Foundation, and NIH grant DC019090 (PFA).

References

Apostolides PF, Milstein AD, Grienberger C, Bittner KC, Magee JC (2016) Axonal Filtering Allows Reliable Output during Dendritic Plateau-Driven Complex Spiking in CA1 Neurons. Neuron 89:770–783.

Bajo VM, Nodal FR, Korn C, Constantinescu AO, Mann EO, Boyden ES, King AJ (2019) Silencing cortical activity during sound-localization training impairs auditory perceptual learning. Nat Commun 10:3075.

Bajo VM, Nodal FR, Moore DR, King AJ (2010) The descending corticocollicular pathway mediates learning-induced auditory plasticity. Nat Neurosci 13:253–260.

Banerjee A, Seriès P, Pouget A (2008) Dynamical constraints on using precise spike timing to compute in recurrent cortical networks. Neural Comput 20:974–993.

Beaulieu-Laroche L, Toloza EHS, Brown NJ, Harnett MT (2019) Widespread and Highly Correlated Somato-dendritic Activity in Cortical Layer 5 Neurons. Neuron 103:235-241.e4.

Bell CC, Han V, Sawtell NB (2008) Cerebellum-like structures and their implications for cerebellar function. Annu Rev Neurosci 31:1–24.

Bieszczad KM, Weinberger NM (2010) Representational gain in cortical area underlies increase of memory strength. Proc Natl Acad Sci U S A 107:3793–3798.

Bittner KC, Grienberger C, Vaidya SP, Milstein AD, Macklin JJ, Suh J, Tonegawa S, Magee JC (2015) Conjunctive input processing drives feature selectivity in hippocampal CA1 neurons. Nat Neurosci 18:1133–1142.

Bittner KC, Milstein AD, Grienberger C, Romani S, Magee JC (2017) Behavioral time scale synaptic plasticity underlies CA1 place fields. Science 357:1033–1036.

Borst JGG (2010) The low synaptic release probability in vivo. Trends Neurosci 33:259–266.

Brainard M, Knudsen E (1993) Experience-dependent plasticity in the inferior colliculus: a site for visual calibration of the neural representation of auditory space in the barn owl. J Neurosci 13:4589–4608.

Clayton KK, Williamson RS, Hancock KE, Tasaka G-I, Mizrahi A, Hackett TA, Polley DB (2021) Auditory Corticothalamic Neurons Are Recruited by Motor Preparatory Inputs. Curr Biol CB 31:310-321.e5.

Doron G, Shin JN, Takahashi N, Drüke M, Bocklisch C, Skenderi S, de Mont L, Toumazou M, Ledderose J, Brecht M, Naud R, Larkum ME (2020) Perirhinal input to neocortical layer 1 controls learning. Science 370:eaaz3136.

Edeline JM, Pham P, Weinberger NM (1993) Rapid development of learning-induced receptive field plasticity in the auditory cortex. Behav Neurosci 107:539–551.

Feldman DE, Brainard MS, Knudsen EI (1996) Newly learned auditory responses mediated by NMDA receptors in the owl inferior colliculus. Science 271:525–528.

Fletcher LN, Williams SR (2019) Neocortical Topology Governs the Dendritic Integrative Capacity of Layer 5 Pyramidal Neurons. Neuron 101:76-90.e4.

Francioni V, Padamsey Z, Rochefort NL (2019) High and asymmetric somato-dendritic coupling of V1 layer 5 neurons independent of visual stimulation and locomotion. eLife 8:e49145.

Galloni AR, Laffere A, Rancz E (2020) Apical length governs computational diversity of layer 5 pyramidal neurons. eLife 9.

Harnett MT, Xu N-L, Magee JC, Williams SR (2013) Potassium Channels Control the Interaction between Active Dendritic Integration Compartments in Layer 5 Cortical Pyramidal Neurons. Neuron 79:516–529.

Huang Y, Heil P, Brosch M (2019) Associations between sounds and actions in early auditory cortex of nonhuman primates. eLife 8:e43281.

Ji W, Suga N, Gao E (2005) Effects of agonists and antagonists of NMDA and ACh receptors on plasticity of bat auditory system elicited by fear conditioning. J Neurophysiol 94:1199–1211.

Kerlin A, Mohar B, Flickinger D, MacLennan BJ, Dean MB, Davis C, Spruston N, Svoboda K (2019) Functional clustering of dendritic activity during decision-making. eLife 8.

Lacefield CO, Pnevmatikakis EA, Paninski L, Bruno RM (2019) Reinforcement Learning Recruits Somata and Apical Dendrites across Layers of Primary Sensory Cortex. Cell Rep 26:2000-2008.e2.

Larkum ME, Wu J, Duverdin SA, Gidon A (2022) The Guide to Dendritic Spikes of the Mammalian Cortex In Vitro and In Vivo. Neuroscience 489:15–33.

Larkum ME, Zhu JJ, Sakmann B (1999) A new cellular mechanism for coupling inputs arriving at different cortical layers. Nature 398:338–341.

Lee J, Rothschild G (2021) Encoding of acquired sound-sequence salience by auditory cortical offset responses. Cell Rep 37:109927.

Lesicko AMH, Angeloni CF, Blackwell JM, De Biasi M, Geffen MN (2022) Corticofugal regulation of predictive coding. eLife 11:e73289.

Levy S, Lavzin M, Benisty H, Ghanayim A, Dubin U, Achvat S, Brosh Z, Aeed F, Mensh BD, Schiller Y, Meir R, Barak O, Talmon R, Hantman AW, Schiller J (2020) Cell-Type-Specific Outcome Representation in the Primary Motor Cortex. Neuron 107:954-971.e9.

Li N, Chen S, Guo ZV, Chen H, Huo Y, Inagaki HK, Chen G, Davis C, Hansel D, Guo C, Svoboda K (2019) Spatiotemporal constraints on optogenetic inactivation in cortical circuits. eLife 8:e48622.

Lisman J (1997) Bursts as a unit of neural information: making unreliable synapses reliable. Trends Neurosci 20:38–43.

Liu B-H, Huberman AD, Scanziani M (2016) Cortico-fugal output from visual cortex promotes plasticity of innate motor behaviour. Nature 538:383–387.

Liu J, Whiteway MR, Sheikhattar A, Butts DA, Babadi B, Kanold PO (2019) Parallel Processing of Sound Dynamics across Mouse Auditory Cortex via Spatially Patterned Thalamic Inputs and Distinct Areal Intracortical Circuits. Cell Rep 27:872-885.e7.

London M, Roth A, Beeren L, Häusser M, Latham PE (2010) Sensitivity to perturbations in vivo implies high noise and suggests rate coding in cortex. Nature 466:123–127.

Miki T, Nakamura Y, Malagon G, Neher E, Marty A (2018) Two-component latency distributions indicate two-step vesicular release at simple glutamatergic synapses. Nat Commun 9:3943.

Morest DK, Oliver DL (1984) The neuronal architecture of the inferior colliculus in the cat: defining the functional anatomy of the auditory midbrain. J Comp Neurol 222:209–236.

Musall S, Kaufman MT, Juavinett AL, Gluf S, Churchland AK (2019) Single-trial neural dynamics are dominated by richly varied movements. Nat Neurosci 22:1677–1686.

Namboodiri VMK, Huertas MA, Monk KJ, Shouval HZ, Hussain Shuler MG (2015) Visually cued action timing in the primary visual cortex. Neuron 86:319–330.

Naud R, Sprekeler H (2018) Sparse bursts optimize information transmission in a multiplexed neural code. Proc Natl Acad Sci 115:E6329–E6338.

Nelson A, Mooney R (2016) The Basal Forebrain and Motor Cortex Provide Convergent yet Distinct Movement-Related Inputs to the Auditory Cortex. Neuron 90:635–648.

Oberle HM, Ford AN, Dileepkumar D, Czarny J, Apostolides PF (2022) Synaptic mechanisms of top-down control in the non-lemniscal inferior colliculus. eLife 10:e72730.

O'Connor DH, Peron SP, Huber D, Svoboda K (2010) Neural activity in barrel cortex underlying vibrissa-based object localization in mice. Neuron 67:1048–1061.

Pachitariu M, Stringer C, Dipoppa M, Schröder S, Rossi LF, Dalgleish H, Carandini M, Harris KD (2016) Suite2p: beyond 10,000 neurons with standard two-photon microscopy. Neuroscience. Available at: http://biorxiv.org/lookup/doi/10.1101/061507 [Accessed June 11, 2021].

Park J, Phillips JW, Guo J-Z, Martin KA, Hantman AW, Dudman JT (2022) Motor cortical output for skilled forelimb movement is selectively distributed across projection neuron classes. Sci Adv 8:eabj5167.

Payeur A, Guerguiev J, Zenke F, Richards BA, Naud R (2021) Burst-dependent synaptic plasticity can coordinate learning in hierarchical circuits. Nat Neurosci.

Penzo MA, Peña JL (2009) Endocannabinoid-mediated long-term depression in the avian midbrain expressed presynaptically and postsynaptically. J Neurosci Off J Soc Neurosci 29:4131–4139.

Pérez-Garci E, Gassmann M, Bettler B, Larkum ME (2006) The GABAB1b isoform mediates long-lasting inhibition of dendritic Ca2+ spikes in layer 5 somatosensory pyramidal neurons. Neuron 50:603–616.

Peters AJ, Lee J, Hedrick NG, O'Neil K, Komiyama T (2017) Reorganization of corticospinal output during motor learning. Nat Neurosci 20:1133–1141.

Pnevmatikakis EA, Soudry D, Gao Y, Machado TA, Merel J, Pfau D, Reardon T, Mu Y, Lacefield C, Yang W, Ahrens M, Bruno R, Jessell TM, Peterka DS, Yuste R, Paninski L (2016) Simultaneous Denoising, Deconvolution, and Demixing of Calcium Imaging Data. Neuron 89:285–299.

Polley DB, Steinberg EE, Merzenich MM (2006) Perceptual learning directs auditory cortical map reorganization through top-down influences. J Neurosci Off J Soc Neurosci 26:4970–4982.

Ranganathan GN, Apostolides PF, Harnett MT, Xu N-L, Druckmann S, Magee JC (2018) Active dendritic integration and mixed neocortical network representations during an adaptive sensing behavior. Nat Neurosci 21:1583–1590.

Raymond JL, Medina JF (2018) Computational Principles of Supervised Learning in the Cerebellum. Annu Rev Neurosci 41:233–253.

Ruediger S, Scanziani M (2020) Learning speed and detection sensitivity controlled by distinct cortico-fugal neurons in visual cortex. eLife 9.

Schneider DM, Nelson A, Mooney R (2014) A synaptic and circuit basis for corollary discharge in the auditory cortex. Nature 513:189–194.

Schoenfeld G, Kollmorgen S, Lewis C, Bethge P, Reuss AM, Aguzzi A, Mante V, Helmchen F (2021) Dendritic integration of sensory and reward information facilitates learning. Neuroscience. Available at: http://biorxiv.org/lookup/doi/10.1101/2021.12.28.474360 [Accessed June 29, 2022].

Schofield BR (2009) Projections to the inferior colliculus from layer VI cells of auditory cortex. Neuroscience 159:246–258.

Scimemi A, Diamond JS (2012) The number and organization of Ca2+ channels in the active zone shapes neurotransmitter release from Schaffer collateral synapses. J Neurosci Off J Soc Neurosci 32:18157–18176.

Sherman SM, Usrey WM (2021) Cortical control of behavior and attention from an evolutionary perspective. Neuron:S0896-6273(21)00462-1.

Slater BJ, Willis AM, Llano DA (2013) Evidence for layer-specific differences in auditory corticocollicular neurons. Neuroscience 229:144–154.

Solyga M, Barkat TR (2021) Emergence and function of cortical offset responses in sound termination detection. eLife 10:e72240.

Stringer C, Pachitariu M, Steinmetz N, Reddy CB, Carandini M, Harris KD (2019) Spontaneous behaviors drive multidimensional, brainwide activity. Science 364:255.

Suga N, Xiao Z, Ma X, Ji W (2002) Plasticity and corticofugal modulation for hearing in adult animals. Neuron 36:9–18.

Sutton RS, Barto AG (2018) Reinforcement learning: an introduction, Second edition. Cambridge, Massachusetts: The MIT Press.

Takahashi H, Magee JC (2009) Pathway interactions and synaptic plasticity in the dendritic tuft regions of CA1 pyramidal neurons. Neuron 62:102–111.

Takahashi N, Ebner C, Sigl-Glöckner J, Moberg S, Nierwetberg S, Larkum ME (2020) Active dendritic currents gate descending cortical outputs in perception. Nat Neurosci 23:1277–1285.

Takahashi N, Oertner TG, Hegemann P, Larkum ME (2016) Active cortical dendrites modulate perception. Science 354:1587–1590.

Tang L, Higley MJ (2020) Layer 5 Circuits in V1 Differentially Control Visuomotor Behavior. Neuron 105:346-354.e5.

Tervo DGR, Hwang B-Y, Viswanathan S, Gaj T, Lavzin M, Ritola KD, Lindo S, Michael S, Kuleshova E, Ojala D, Huang C-C, Gerfen CR, Schiller J, Dudman JT, Hantman AW, Looger LL, Schaffer DV, Karpova AY (2016) A Designer AAV Variant Permits Efficient Retrograde Access to Projection Neurons. Neuron 92:372–382.

Trautmann EM et al. (2021) Dendritic calcium signals in rhesus macaque motor cortex drive an optical brain-computer interface. Nat Commun 12:3689.

Tsodyks MV, Markram H (1997) The neural code between neocortical pyramidal neurons depends on neurotransmitter release probability. Proc Natl Acad Sci 94:719–723.

Usrey WM, Sherman SM (2019) Corticofugal circuits: Communication lines from the cortex to the rest of the brain. J Comp Neurol 527:640–650.

Williamson RS, Polley DB (2019) Parallel pathways for sound processing and functional connectivity among layer 5 and 6 auditory corticofugal neurons. eLife 8:e42974.

Winer JA, Larue DT, Diehl JJ, Hefti BJ (1998) Auditory cortical projections to the cat inferior colliculus. J Comp Neurol 400:147–174.

Xiong Q, Znamenskiy P, Zador AM (2015) Selective corticostriatal plasticity during acquisition of an auditory discrimination task. Nature 521:348–351.

Xu N, Harnett MT, Williams SR, Huber D, O'Connor DH, Svoboda K, Magee JC (2012a) Nonlinear dendritic integration of sensory and motor input during an active sensing task. Nature 492:247–251.

Xu W, Morishita W, Buckmaster PS, Pang ZP, Malenka RC, Südhof TC (2012b) Distinct neuronal coding schemes in memory revealed by selective erasure of fast synchronous synaptic transmission. Neuron 73:990–1001.

Yan W, Suga N (1998) Corticofugal modulation of the midbrain frequency map in the bat auditory system. Nat Neurosci 1:54–58.

Yudintsev G, Asilador AR, Sons S, Vaithiyalingam Chandra Sekaran N, Coppinger M, Nair K, Prasad M, Xiao G, Ibrahim BA, Shinagawa Y, Llano DA (2021) Evidence for Layer-Specific Connectional Heterogeneity in the Mouse Auditory Corticocollicular System. J Neurosci Off J Soc Neurosci 41:9906–9918.

Zhang LI, Bao S, Merzenich MM (2001) Persistent and specific influences of early acoustic environments on primary auditory cortex. Nat Neurosci 4:1123–1130.

Znamenskiy P, Zador AM (2013) Corticostriatal neurons in auditory cortex drive decisions during auditory discrimination. Nature 497:482–485.

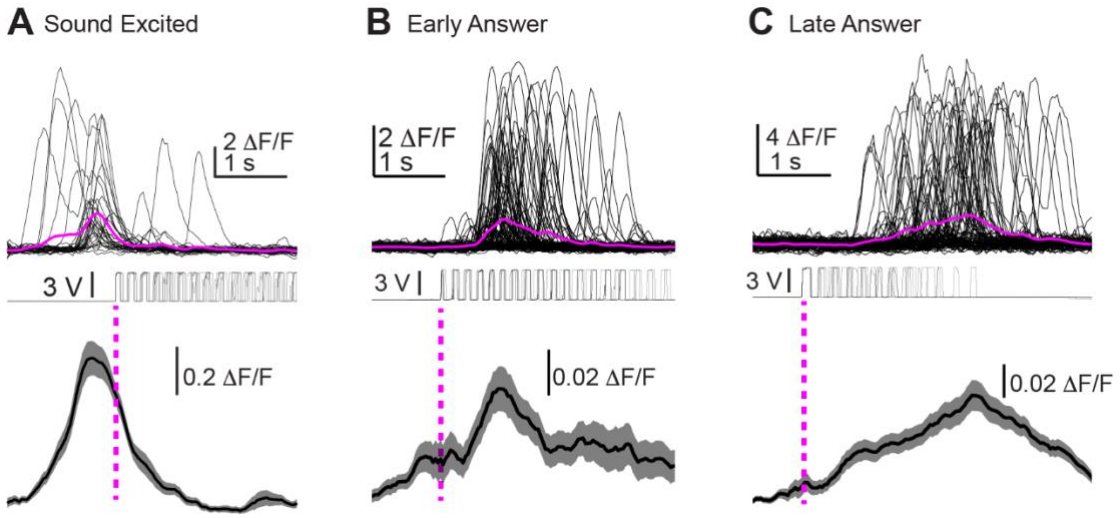

Supplemental Figure 1: *Differential latencies of sound- and answer-modulated dendrites relative to licking onset.* **A)** Upper panel: Individual fluorescence traces (black) and across-trial average (magenta) aligned to the first lick for a sound excited dendrite. Middle panel: Digitized output of the optical lick detector used for alignment of traces. Lower panel: Population average of lick-aligned fluorescence across the population of sound-excited dendrites. Of note is that the fluorescence peaks prior to first lick onset. Panels B-C: Same as A, but for early (**B**) and late (**C**) answer responsive dendrites.

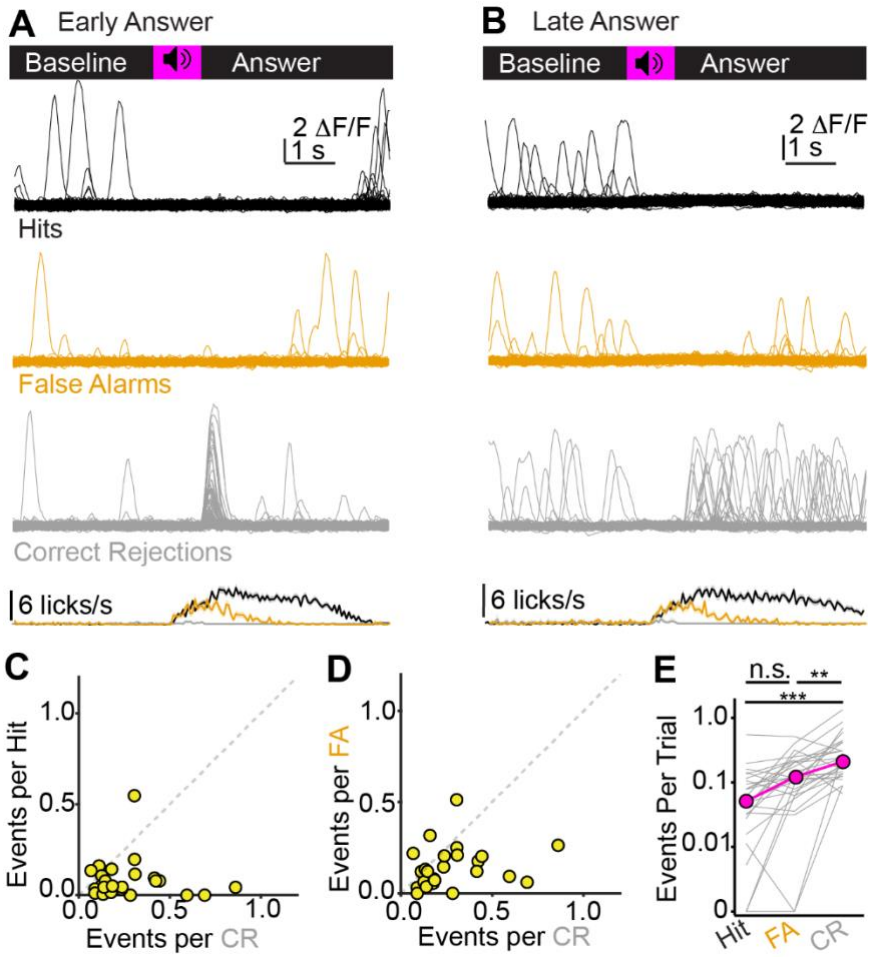

Supplemental Figure 2: *NO-GO selective, answer responsive dendrites are preferentially active on correct rejection trials.* **A)** Overlaid fluorescence traces and lick rate histogram for a NO-GO selective, early answer responsive dendrite on hits, false alarms, and correct rejections. This ROI was recorded in the same session as the example early answer dendrite in 3B, such that the behavioral traces are identical. **B)** Same as panel A, but for a NO-GO selective late answer responsive dendrite. Of note in A and B is that the increase in dendritic Ca^{2+} spikes during the answer period does not occur on false alarm trials. **C)** Number of dendritic spikes on hits and correct rejections (y and x axes, respectively) are plotted for n = 26 NO-GO selective, answer responsive dendrite. **D)** Same as C, but for false alarms and correct rejections. Of note is that most datapoints fall below the unity line in both panels, indicating selective activity on correct rejections. **E)** Summary data showing the number of events per trial for each outcome category in n = 26 NO-GO selective, answer responsive dendrites. Median event probability: 5.0, 12.2, and 18.5% for hits, false alarms, and correct rejections, respectively (Magenta points and line). $F(3,31)=28.31$, $p<0.0001$, Friedman test. $P<0.01$ comparing correct rejections vs hits or false alarms, $p=0.0925$ hits vs false alarms, Dunn's post-hoc tests). Of note, y-axis is a log scale. Asterisks denote statistical significance.

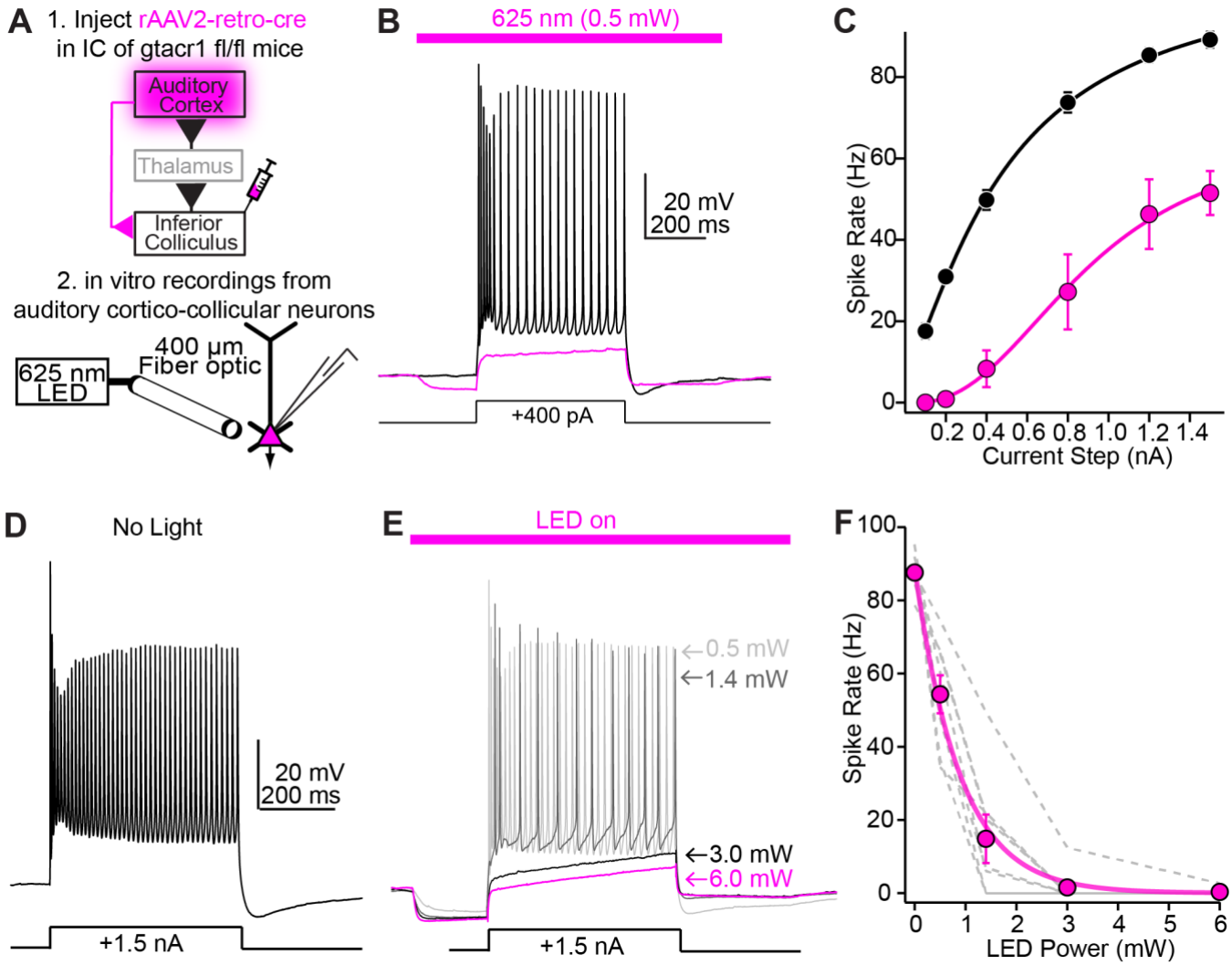

Supplemental Figure 3: *GtACR1 activation silences auditory corticofugal neurons.* **A)** Cartoon of experiment. Retrograde-cre is injected in the IC of GtACR1 fl/fl mice. Whole-cell patch clamp recordings are obtained ~2 weeks later from GtACR1 expressing corticofugal layer 5 neurons in acute auditory cortex brain slices. GtACR1 is activated via a 625 nm coupled optic fiber positioned above the slice. **B)** Example recording showing spike responses to 400 pA current steps in absence or presence of GtACR1 activation (0.5 mW; black and magenta traces, respectively). **C)** Summary data of FI curves in absence or presence of GtACR1 activation (n = 9 cells from N = 2 mice). Color scheme is same as panel B. Lines are Hill fits. Main effect of current step: $F(5,40)=89.62$; Main effect of Light: $F(1,8)= 71.63$; Light x current interaction: $F(5,28)=6.494$, all $p<0.001$, mixed effects model. **D,E)** Example traces showing spike responses during 1.5 nA current step in absence (D) or presence (E) of different light levels. **F)** Summary showing the effect of increasing light levels on spike rates during 1.5 nA current steps (n=8 cells from N = 2 mice). Of note is the near complete absence of spiking with >3 mW light. Gray lines are individual neurons, magenta points are mean ± SEM. Magenta line is mono-exponential fit to mean data.